TU Delft

Delft University of Technology

Anisotropic proximity-induced superconductivity and edge supercurrent in Kagome metal, $K_{1-x}V_3Sb_5$

Wang, Yaojia; Yang, Shuo Ying; Sivakumar, Pranava K.; Ortiz, Brenden R.; Teicher, Samuel M.L.; Wu, Heng; Srivastava, Abhay K.; Garg, Chirag; Ali, Mazhar N.; More Authors

DOI
10.1126/sciadv.adg7269

Publication date
2023

Document Version
Final published version

Published in
Science Advances

Citation (APA)
Wang, Y., Yang, S. Y., Sivakumar, P. K., Ortiz, B. R., Teicher, S. M. L., Wu, H., Srivastava, A. K., Garg, C., Ali, M. N., & More Authors (2023). Anisotropic proximity-induced superconductivity and edge supercurrent in Kagome metal, $K_{1-x}V_3Sb_5$. *Science Advances*, *9*(28), eadg7269. Article eadg7269. https://doi.org/10.1126/sciadv.adg7269

Important note
To cite this publication, please use the final published version (if applicable).
Please check the document version above.

Copyright
Other than for strictly personal use, it is not permitted to download, forward or distribute the text or part of it, without the consent of the author(s) and/or copyright holder(s), unless the work is under an open content license such as Creative Commons.

Takedown policy
Please contact us and provide details if you believe this document breaches copyrights.
We will remove access to the work immediately and investigate your claim.

This work is downloaded from Delft University of Technology.
For technical reasons the number of authors shown on this cover page is limited to a maximum of 10.

MATERIALS SCIENCE

Anisotropic proximity–induced superconductivity and edge supercurrent in Kagome metal, $K_{1-x}V_3Sb_5$

Yaojia Wang[1,2]*, Shuo-Ying Yang[1], Pranava K. Sivakumar[1], Brenden R. Ortiz[3], Samuel M. L. Teicher[3], Heng Wu[1,2], Abhay K. Srivastava[1], Chirag Garg[1,4], Defa Liu[1,5], Stuart S. P. Parkin[1], Eric S. Toberer[6], Tyrel McQueen[7], Stephen D. Wilson[3], Mazhar N. Ali[1,2]*

Copyright © 2023 The Authors, some rights reserved; exclusive licensee American Association for the Advancement of Science. No claim to original U.S. Government Works. Distributed under a Creative Commons Attribution License 4.0 (CC BY).

Materials with Kagome nets are of particular importance for their potential combination of strong correlation, exotic magnetism, and electronic topology. KV_3Sb_5 was discovered to be a layered topological metal with a Kagome net of vanadium. Here, we fabricated Josephson Junctions of $K_{1-x}V_3Sb_5$ and induced superconductivity over long junction lengths. Through magnetoresistance and current versus phase measurements, we observed a magnetic field sweeping direction–dependent magnetoresistance and an anisotropic interference pattern with a Fraunhofer pattern for in-plane magnetic field but a suppression of critical current for out-of-plane magnetic field. These results indicate an anisotropic internal magnetic field in $K_{1-x}V_3Sb_5$ that influences the superconducting coupling in the junction, possibly giving rise to spin-triplet superconductivity. In addition, the observation of long-lived fast oscillations shows evidence of spatially localized conducting channels arising from edge states. These observations pave the way for studying unconventional superconductivity and Josephson device based on Kagome metals with electron correlation and topology.

INTRODUCTION

The Kagome lattice, formed by corner-sharing triangles of atoms, is an important structure type that is proximate to the honeycomb (like graphene), hosting topological band structures, electron correlation, and geometrical frustration (*1*–*3*). It is an ideal platform for investigating many exotic electronic behaviors such as the quantum spin liquid state, unconventional superconductivity, and Dirac/Weyl/Nodal line semimetal behavior (*3*–*6*). Recently, the family of Kagome metals AV_3Sb_5 (A = K, Cs, and Rb) (*7*) has attracted substantial attention due to the observation of diverse physical properties including charge-density waves (CDWs) (*8*–*13*), superconductivity (*14*–*17*), a giant anomalous Hall effect (AHE) (*18*, *19*), and topological states (*14*, *18*, *20*, *21*).

Many studies have been performed to explore and understand the nature of these properties and electronic states in the AV_3Sb_5 quantum material family. While no long-range magnetic order has been observed through inelastic neutron scattering (*7*), muon spin relaxation experiments have shown signals of time-reversal symmetry (TRS) breaking with weak internal local magnetic field below CDW transition in KV_3Sb_5 and CsV_3Sb_5 (*22*–*24*). This aligned well with the observed giant extrinsic skew scattering AHE below the CDW transition (*18*, *19*). In addition, chiral charge ordering with magnetic field tunability and charge order states breaking rotation symmetry were detected in CsV_3Sb_5 and KV_3Sb_5 (*9*, *11*, *12*, *25*–*27*), and possible unconventional superconductivity in AV_3Sb_5 was also discussed (*11*, *12*, *22*, *28*). Theoretically, several ground states of AV_3Sb_5 were proposed including a star-of-David structure, tri-hexagonal structures, and TRS breaking states such as a chiral flux state, charge/spin bond orders, spin density waves, and excitonic order (*29*–*35*). However, differing reports on the presence or absence of these order states and the nature of the superconductivity (*25*, *36*–*38*) has made understanding the magnetism and superconductivity in the AV_3Sb_5 family difficult, and there is a lot of space to excavate the underlying physics.

In addition to looking for intrinsic superconductivity, using the proximity effect is another route to investigate the superconducting and electronic properties of materials. The quantum material Josephson junction (JJ), where two superconductors (SC) are coupled via a bridge of nonsuperconducting (non-SC) quantum material, is an effective structure to induce superconductivity. In a JJ, proximity-induced Cooper pairs are very sensitive to the barrier properties, and the resultant interference effects based on the coupling of the SC wave functions can reveal inherent physical properties of the barriers, including topological states and magnetism (*39*–*41*). On the other hand, the JJ is an important structure to explore intriguing physical properties, such as generating spin-triplet Cooper pairs in JJs of magnetic barriers (*42*–*49*) and exploring possible topological superconductivity through superconductivity of a topological state (*50*, *51*). Thus, JJs with topological Kagome metal barriers are a great tool to explore intriguing superconducting properties and understand the physical properties of Kagome materials.

In this work, we fabricated JJs of intrinsically non-SC, potassium-deficient $K_{1-x}V_3Sb_5$ ($x \sim 0.26$ to 0.31) and then induced superconductivity through proximity. The Josephson effect is observed in long channels up to 6 μm, and the JJs exhibit a prominent asymmetry and reversion of the magnetoresistance for the up and down magnetic field sweeps only in the superconducting state of the JJ. Moreover, the interference pattern of critical current (I_c) versus magnetic field shows a typical Fraunhofer-like pattern for an applied in-plane field but an anomalous pattern with a minimum near-zero field for an applied out-of-plane field. These unusual

[1]Max Planck Institute of Microstructure Physics, 06108 Halle, Saxony-Anhalt, Germany. [2]Kavli Institute of Nanoscience, Delft University of Technology, Delft, The Netherlands. [3]Materials Department, University of California Santa Barbara, Santa Barbara, CA 93106, USA. [4]IBM Almaden Research Center, San Jose, CA 95120, USA. [5]Department of Physics, Beijing Normal University, Beijing 100875, China. [6]Colorado School of Mines, Goldon, CO 80401, USA. [7]Johns Hopkins University, Baltimore, MD 21218, USA.
*Corresponding author. Email: whyjwang@gmail.com (Y.W.); maz@berkeley.edu (M.N.A.)

Downloaded from https://www.science.org at Delft University on July 24, 2023

magnetic field modulations of supercurrent with strong directional anisotropy indicate that the superconducting coupling in the junction is influenced by the internal anisotropy of $K_{1-x}V_3Sb_5$, which should be related to the charge order state and the internal magnetic field. The possible spin-triplet pairing in the JJs is discussed. Last, a nonvanishing, fast oscillation of I_c with a scalloped peak profile and excitation branches was observed, indicating the presence of edge localized supercurrent. Theoretical analysis of the band structure confirms the expectation of topological surface states in the (010)/(100) plane of KV_3Sb_5, corresponding to the edges of our samples. This solidifies $K_{1-x}V_3Sb_5$ as an exciting platform to study the interplay of superconductivity, unconventional charge order state, and topology and also to show the potential of Kagome materials JJ for exploring unconventional superconductivity.

RESULTS

Proximity effect–induced superconductivity

KV_3Sb_5 crystallizes in the hexagonal centrosymmetric space group *P6*/mmm and is composed of Kagome layers of vanadium interleaved with honeycomb layers of Sb and K (Fig. 1A). JJs with different channel lengths were fabricated on $K_{1-x}V_3Sb_5$ nanoflakes with Nb [critical temperature (T_c) ~ 6 K] as the superconducting electrodes. The nanoflakes were exfoliated from the same batch of crystals used in the work of Yang *et al.* (*18*), which were grown using the same method as previously described by Ortiz *et al.* (*7*). It should be noted that, although stoichiometric KV_3Sb_5 can intrinsically superconduct (*15*), the potassium-deficient $K_{1-x}V_3Sb_5$ flakes can be non-SC. We fabricated $K_{1-x}V_3Sb_5$ devices with Au contacts to study the intrinsic properties at ultralow temperatures. Superconductivity was observed in some Au devices with T_c ~ 0.6 to 0.65 K and I_c ~ 13 to 18 μA but was absent in others. Using electron-dispersive x-ray spectroscopy measurements, it was revealed that there were different compositions in the superconducting Au-contacted samples compared with the non-SC samples; the superconducting samples were closer to the ideal 1:3:5 stoichiometry compared to the non-SC samples (see details in section S3), which is consistent with the observation of intrinsic superconductivity in stoichiometric bulk KV_3Sb_5 with a maximum T_c ~ 0.93 K (*15*). The reduced T_c in the deficient samples compared with stoichiometric KV_3Sb_5 and the disappearance of superconductivity in our $K_{1-x}V_3Sb_5$ samples with low-potassium concentration indicate that the superconductivity in KV_3Sb_5 is highly dependent on defect/doping. In this work, the non-SC $K_{1-x}V_3Sb_5$ samples with highly potassium deficiency (x = 0.26 to 0.31) were used to fabricate the JJs.

Figure 1B shows a schematic structure of a Nb/$K_{1-x}V_3Sb_5$/Nb device and one of the fabricated devices with channel length L varying from 0.1 to 6.05 μm with a constant sample thickness of ~45 nm (device #1). We first measured R versus T curves of both short (L = 0.1 μm) and intermediate channels (L = 1.88 μm) by the four-probe method to exclude the contact resistance (results shown in Fig. 1C). A sudden drop in resistance is observed at temperatures of 0.76 and 0.68 K for channels of L = 0.1 and 1.88 μm, respectively, with the same artifactual residual resistance value from lock-in measurements (see discussion in section S1). The I versus V curves measured at ~20 mK show a sudden jump in voltage above I_c, further confirming the superconducting state at low temperature (Fig. 1C, inset).

To verify that the superconducting signal is related to the proximity effect from the superconducting electrodes, we investigated the length dependence of superconductivity by measuring the I versus V curves of different channel lengths at 20 mK using the two-probe method. Figure 2A shows the results measured in device #1; the superconducting transition is observed up to 6.05 μm. The extracted I_c (taken from the peak location on dV/dI versus I curve) is small (I_c < 1 μA) and different for different channel lengths, consistent with proximity-induced superconductivity. Unexpectedly, I_c increases with increasing channel length (Fig. 2B, red dashed line), distinct from a typical JJ with a transparent interface in which I_c monotonically reduces with increasing channel length (at fixed thickness and width) due to reduced coupling between the two superconducting electrodes (*52*). However, because the contact resistance of the interface is higher than the sample resistance in our device, the interface of each channel needs to be considered. We extracted the I_cR_N of different JJs, where R_N is the normal state resistance of the junction. As shown in Fig. 2B (purple dashed line), I_cR_N varies weakly with channel length, indicating that the I_c is being dominated by the interface

Downloaded from https://www.science.org at Delft University on July 24, 2023

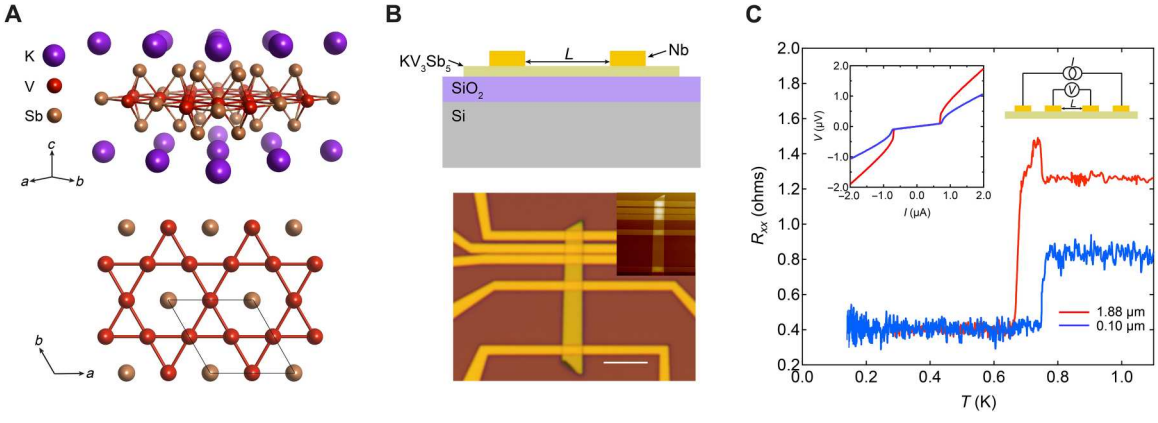

Fig. 1. Crystal structure and JJ of KV_3Sb_5. (**A**) Top: Crystal structure of KV_3Sb_5. Bottom: Projection along the *c* axis showing the Kagome net of vanadium. (**B**) Top: Side-view schematic of $K_{1-x}V_3Sb_5$ JJ. Bottom: The optical and atomic force microscopy (inset) image of one fabricated JJ device (device #1) of $K_{1-x}V_3Sb_5$ thin flake (~ 45 nm). Scale bar, 5 μm. (**C**) Superconducting transition of device #1 measured by four-probe method. The insets are schematic of measurement circuit (top right) and typical voltage versus current curves measured at 20 mK (top left).

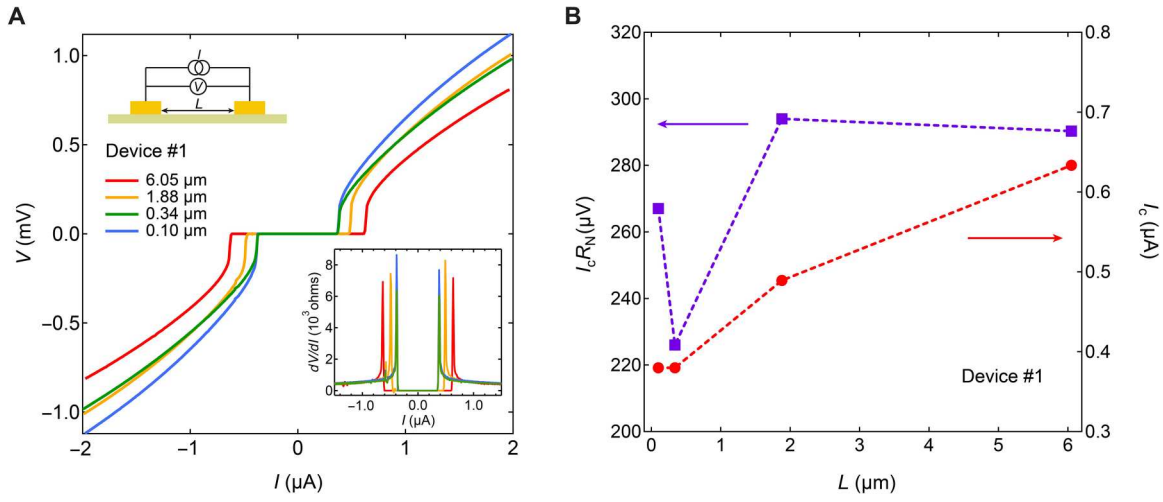

Fig. 2. Length dependence of Josephson current. (**A**) Voltage versus current (*V-I*) curves for different channel lengths measured by two-probe method at 20 mK. The insets are corresponding differential resistance (down right) and schematic of measurement circuit (top left). (**B**) Length dependent I_c and I_cR_N extracted from the *V-I* curves in (A).

of the SC with the $K_{1-x}V_3Sb_5$ barrier; similar I_cR_N are also observed in other devices (see results of device #2 in section S2). This again shows that the supercurrent is induced by the proximity effect of the superconducting electrodes.

The proximity effect–induced superconductivity is also supported by many other pieces of evidence. The superconducting transition temperatures and I_c of different junctions made on the same flake (with uniform width and thickness) are different (Figs. 1C and 2), which is fundamentally distinct from an intrinsically superconducting flake with uniform width and thickness that would have constant T_c and I_c. In addition, we compare the magnetic field dependence of the resistance and I_c (discussed in detail later) in highly potassium-deficient $Nb/K_{1-x}V_3Sb_5/Nb$ junction (Figs. 3 and 4) with Au-contacted superconducting $K_{1-x}V_3Sb_5$ sample (fig. S4). A Fraunhofer pattern was observed (Fig. 4A) in the Nb-contacted junction but disappeared in the Au-contacted superconducting sample (fig. S4), which is a strong evidence for Josephson coupling in our $Nb/K_{1-x}V_3Sb_5/Nb$ junction, and against intrinsic superconductivity. Moreover, the critical field (B_c) of superconductivity in the Nb-contacted junction (e.g., B_c ~ 300 mT for in-plane field and ~ 85 mT for out-of-plane field for L = 6.05 μm) is much higher than that in the intrinsic Au-contacted superconducting $K_{1-x}V_3Sb_5$ (~100 mT for in-plane field, and ~15 to 20 mT for out-of-plane field). The Fraunhofer pattern also sustains up to ~300 mT (Fig. 4A) for in-plane field. These results strongly indicate that the superconductivity in Nb-contacted junctions is coming from the proximity effect of superconducting electrodes. In addition, the contribution of inhomogeneous superconductivity in the junction can also be excluded. A more comprehensive discussion of the proximity effect–induced superconductivity is included in section S4.

While the proximity length up to 6.05 μm is quite long, much longer than the coherence length (ξ_N~230 nm) calculated on the basis of bulk mobility of the barrier material (see details in

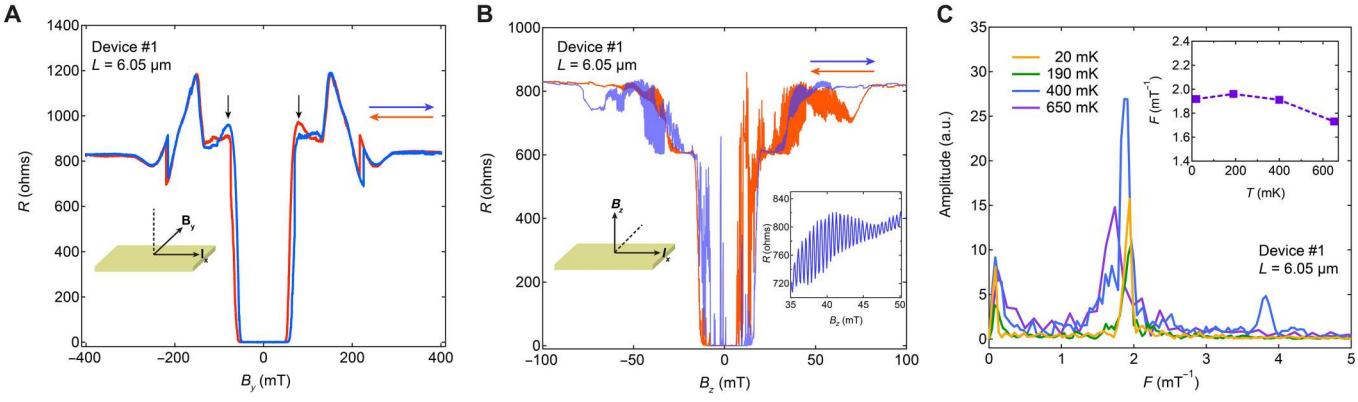

Fig. 3. Magnetic field–dependent resistance of JJ with L = 6.05 μm. (**A**) *R* versus *B* with magnetic field applied in-plane but orthogonal to the current. Red (blue) line and arrows denote field downsweeping (upsweeping). The two black arrows point out the reversion of resistance for different sweep directions. The inset denotes magnetic field and current directions. (**B**) *R* versus *B* of the same device with magnetic field applied out of plane and orthogonal to the current. The left inset denotes magnetic field and current directions, and the right inset is the enlarged plot of fast oscillation. (**C**) Fast Fourier transform of fast oscillation in (B) at different temperatures; the inset is temperature-dependent oscillation frequency obtained in the main panel of (C). a.u., arbitrary units.

Downloaded from https://www.science.org at Delft University on July 24, 2023

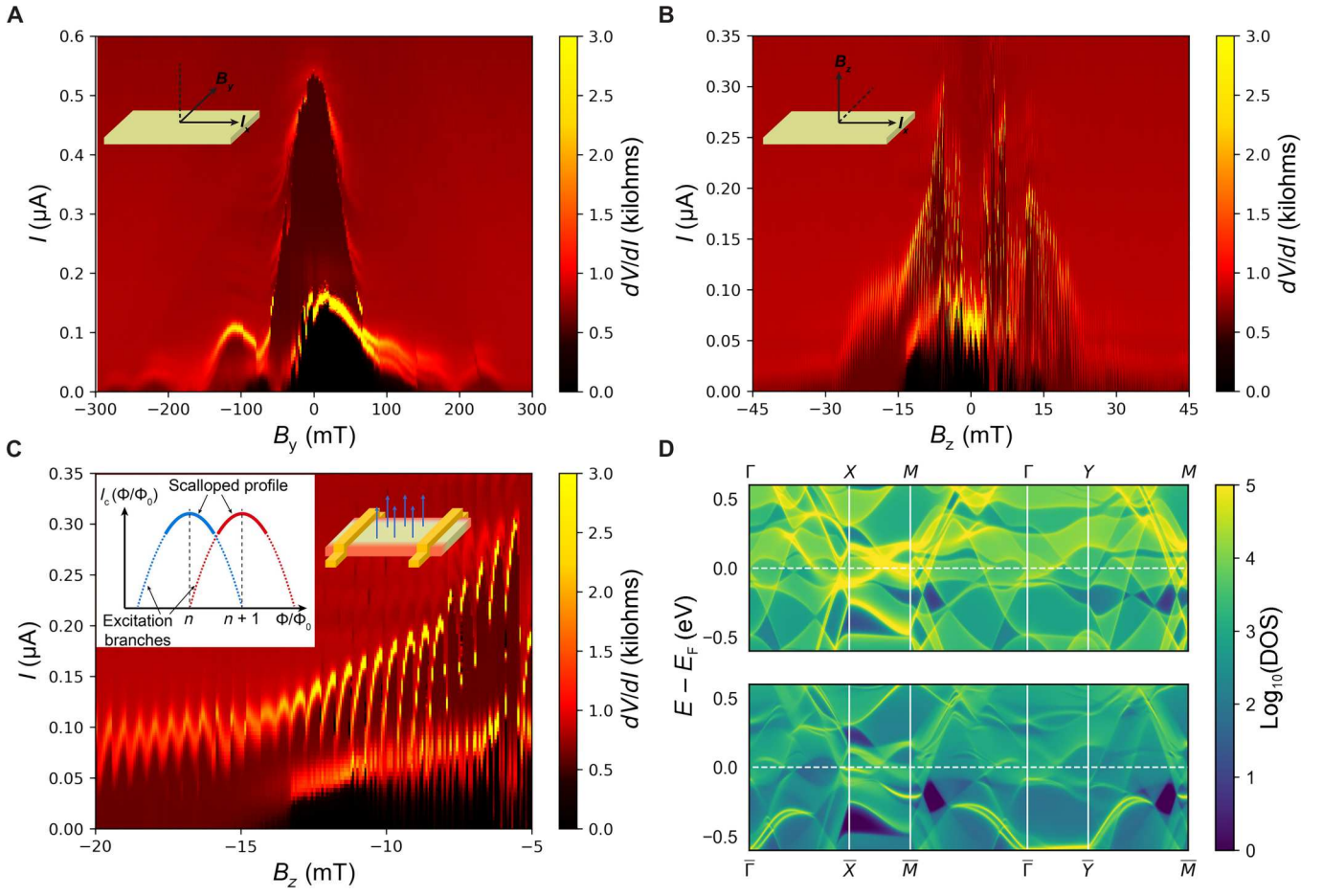

Fig. 4. Interference patterns and localized Josephson current. (**A** and **B**) Color maps of *dV*/*dI* versus current and magnetic field measured in device #1 at 20 mK when applying in-plane magnetic field and out-of-plane magnetic field, respectively. The field is changing from positive to negative during the measurement. The insets denote magnetic field and current directions. (**C**) Main panel: The enlarged plots of the fast oscillation in (B) when applying out-of-plane field. The right inset is a schematic of the edge supercurrent in the JJ, the edges are indicated by red color. The left inset is a schematic current profile of an edge state. (**D**) Top: Bulk spectral density of states (DOS) for KV_3Sb_5 on the (010)/(100) surfaces. Bottom: Surface spectral density of states for the (010)/(100) surfaces. Several bright bands are present in the bottom panel but not in the top panel; these are the surface states.

Methods), similar results have been observed in JJs with a giant proximity effect when the non-SC bridge material in a JJ is close to superconducting itself (i.e., can superconduct with mild doping or temperature is above T_c of barrier) (*53*, *54*) or in topological materials with topological edge/surface states (*55*, *56*). Because stoichiometric KV_3Sb_5 can be an intrinsic SC, the $K_{1-x}V_3Sb_5$ sample in the JJ may be relatively near a superconducting state and helping create the long Josephson length. This may also be the reason of weaker length dependence of superconductivity in our junction compared with typical JJs. In addition, the topological properties of $K_{1-x}V_3Sb_5$ (addressed below) may also contribute to the observed long junction lengths.

Magnetic field sweep direction dependence of magnetoresistance

We next study the magnetic field dependence of superconductivity in the $K_{1-x}V_3Sb_5$ JJs with both in-plane and out-of-plane magnetic field. Figure 3 shows the results of the channel with $L = 6.05$ μm in device #1. When applying the magnetic field (labeled B_y) in the sample plane perpendicular to the current direction (labeled I_x) at 20 mK, the breaking of superconductivity is observed at an in-plane B_c of ~300 mT (Fig. 3A). In particular, the R versus B curve is asymmetric about zero field for positive and negative field, but the curve reverses for upsweep (blue line) and downsweep (red line) of the field, as indicated by the black arrows in Fig. 3A. This property is also observed when applying an out-of-plane magnetic field (B_z direction). As shown in Fig. 3B, the R versus B curves at 20 mK present a prominent asymmetry and reversion for upsweep and downsweep with an out-of-plane B_c of ~85 mT. This flipping property of the R versus B curves is observed in all the measured $K_{1-x}V_3Sb_5$ JJs and channels for both in-plane and out-of-plane fields (see more data for other channels in fig. S6). Moreover, Fig. 3B presents a prominent fast oscillation overlaid on the background of the R versus B. Using fast Fourier transform analysis, the frequency of fast oscillation is extracted and found to be 1.9 mT^{-1} and is not sensitive to temperature until very near the superconducting transition, as shown in Fig. 3C (additional data in fig. S9). This robust fast oscillation is related to the interference of supercurrent and is modulated by the magnetic flux, like a superconducting quantum interference device (SQUID), and its origin is discussed in detail below. Similar

Downloaded from https://www.science.org at Delft University on July 24, 2023

to the background of the R versus B curves, the fast oscillation also reverses for different field sweep directions (Fig. 3B).

Anisotropic interference pattern for in-plane and out-of-plane magnetic field

To further understand the magnetic field dependence of superconductivity, the magnetic field modulation of the critical supercurrent in the $K_{1-x}V_3Sb_5$ JJs is studied. Figure 4 (A and B) is the color maps of dV/dI versus I and B for in-plane field and out-of-plane field, respectively, measured by downsweep of the field for the 6.05-μm JJ (see fig. S8 in for upsweep pattern). There are two sets of interference patterns (bright lines) on the color maps, which may be indicative of distinct superconducting channels in the $K_{1-x}V_3Sb_5$ JJ (see detailed discussion in section S8). Because the outside pattern sustains to higher field than the inside pattern and dominates the primary interference features, we focus on the outside pattern. When applying the in-plane magnetic field, with $B_y \perp I_x$, the main interference pattern of I_c versus B shows a prominent peak at zero field, and the oscillation of I_c decays quickly with increasing field, as is expected of a Fraunhofer-like I_c versus B pattern for a JJ. This confirms that Josephson coupling is achieved in these devices. However, when applying an out-of-plane (B_z) magnetic field (Fig. 4B), the interference pattern shows an anomalous suppression near-zero field, resulting in a minimum instead of a peak, at the center of the interference pattern. Under a weak magnetic field (either up or down), the I_c is enhanced relative to zero field but is still smaller than the maximum I_c with in-plane field. This anisotropic interference pattern and suppression of I_c are quite unusual. In addition, a long-lived fast, SQUID-like oscillation is also clearly visible on top of the primary background in Fig. 4B. Because the superconductivity presents many properties, we discuss these properties piecewise and their related physical origins in detail below.

DISCUSSION

Anisotropic internal magnetic field and spin-triplet superconductivity

The results in Figs. 3 and 4 show the distinct magnetic field dependence of superconductivity in a $K_{1-x}V_3Sb_5$ JJ including the reversion of the R versus B curves when changing field sweeping direction and anisotropic interference patterns with central peak for in-plane field but abnormal suppression of I_c for out-of-plane field. These features are also observed in the superconducting state of other Nb-contacted $K_{1-x}V_3Sb_5$ junctions (figs. S5 and S6) but disappear in Au-contacted superconducting devices (see details in fig. S4), indicating that they are properties of the proximity-induced supercurrent in the JJs.

In KV_3Sb_5, no long-range magnetic order has been observed down to 0.25 K via neutron scattering (below the T_c of these JJs) (*7*); however, it has presented large AHE, and a signal of TRS breaking with weak internal local magnetic field was detected below the CDW transition via muon spin relaxation (*22*); similar TRS breaking below CDW is also widely observed in its sister materials CsV_3Sb_5 (*23*, *57*) and RbV_3Sb_5 (*58*). We note that the signal of CDW transition and AHE also appear in our non-JJ, Au-contacted non-SC $K_{1-x}V_3Sb_5$ samples (see data in fig. S3), which indicates that the TRS breaking with internal magnetic field is preserved in our potassium-deficient samples. In JJs, the internal magnetic field of the barrier will influence the injection and transport of Cooper pairs (*42*), which can lead to the reversion of R versus B curves, as has been widely observed in JJs with barrier materials breaking TRS, such as ferromagnets (*59*) and magnetic element–doped barriers (*49*). The reversion of magnetoresistance is robustly observed in all $K_{1-x}V_3Sb_5$ JJs with different channel lengths, indicating that it is an intrinsic property that should be induced by the internal local magnetic field in $K_{1-x}V_3Sb_5$. As a control, we also fabricated the Nb/graphene/Nb JJ, and the reversion feature is absent, as expected (see data of a Nb/graphene/Nb JJ in fig. S7).

The distinct interference patterns for in-plane and out-of-plane field in $K_{1-x}V_3Sb_5$ JJ imply that the internal field is also anisotropic, as the superconducting coupling in the junction was modulated differently when changing the direction of the external magnetic field. Recently, muon spin relaxation experiments have reported anisotropy of the internal local magnetic field between in-plane and out-of-plane directions in the sister compound CsV_3Sb_5 (*23*). The emergence of local internal field was found to be associated with the charge order transition (*23*, *24*). So far, the low-temperature order states in KV_3Sb_5 and CsV_3Sb_5 are still not clear, with several types of charge/spin orders breaking TRS having been proposed, including a chiral flux phase (*32*), charge/spin bond order (*29*, *34*), and spin density wave (*31*). Note that the easy plane of these orders lies in-plane (Kagome lattice), and it was also proposed that the out-of-plane magnetic field (along the c axis) can modulate these orders (*31*), and obvious enhancement of the magnetic field signal under out-of-plane field was detected in muon and optical experiments (*23*, *57*). The field modulatable ordered states and related internal magnetic field likely contribute to the anisotropic magnetic field response of supercurrent in the JJ.

Associated with this anisotropic magnetic field dependence of the supercurrent, we discuss the origin of the suppressed I_c with a minimum near-zero field in the interference pattern (out-of-plane field). In general, a JJ with normal spin-singlet pairing of nonmagnetic barriers displays a standard single-slit Fraunhofer interference pattern, with periodic oscillations and a central maximum. The unusual central minimum of I_c normally appears in JJs with magnetic barriers where the junction has modulated phase and spin-triplet paring (*42*, *60*). A very similar suppression and minimum of I_c was observed in JJs with long range spin-triplet pairing, such as the JJ of half-metal CrO_2 and in hybrid superconductor/ferromagnet junctions (*45*, *61*). The conversion of spin singlet to triplet pairing in JJs generally happens on the basis of inhomogeneous magnetizations, noncollinear spin structures, or spin spiral structures, which breaks spin rotation symmetry allowing spin-flipping at the interfaces (*42*, *44*, *47*).

For the KV_3Sb_5 family, as discussed before, TRS breaking was reported in many works, and several possible charge/spin order states were predicted in the Kagome plane (*23*, *29*, *31*, *32*, *34*, *57*), which can be modulated by external out-of-plane magnetic field (*23*, *31*, *57*), and many experiments have detected an enhanced magnetic field signal under this field direction (*23*, *57*). Among these, one widely discussed order is chiral charge order with loop current, which induces a varying local magnetic field (dependent on the hexagons versus triangles) in Kagome lattices (*24*, *32*, *57*). Other predicted spin orders also have varying spin directions (*29*, *31*, *62*). In addition, rotation symmetry breaking in KV_3Sb_5 (*25*) was also reported at low temperatures in scanning tunneling microscopy study. These broken symmetries combined with the spatial variation of local internal magnetic field make it possible to convert

Downloaded from https://www.science.org at Delft University on July 24, 2023

spin-singlet to spin-triplet supercurrent in $K_{1-x}V_3Sb_5$ JJs and allow modulation of the superconducting coupling when the out-of-plane field tunes the ordered state and internal field. This also aligns with theoretical studies that found that both spin-singlet and spin-triplet pairing can appear in the KV_3Sb_5 family due to the complex band structure and electron correlations (particularly as a function of Fermi level that can be modulated by doping) (*28*, *63*, *64*) and that triplet pairing may be a favored state in the (relatively) weak correlation region (*28*). The combination of the observed abnormal interference pattern and these inherent properties of $K_{1-x}V_3Sb_5$ indicates that spin-triplet pairing is possible in $K_{1-x}V_3Sb_5$ JJs, and more experimental effort in future, including elucidation of the ground state in the AV_3Sb_5 family, will help understand the superconducting behavior in $K_{1-x}V_3Sb_5$ JJs.

Supercurrent of edge state

We next analyze the oscillations in the interference pattern and focus on the spatial distribution of the supercurrent and the prominent long-lived fast, SQUID-like oscillation of I_c in the Fig. 4. In the junction, the I_c is modulated by the magnetic flux in units of the flux quantum Φ_0 with $\Phi_0 = \Delta B \cdot L \cdot t_{eff}$ ($L \approx 6.05$ μm). On the basis of the Fraunhofer-like pattern (period of $\Delta B \sim 100$ mT) for the in-plane magnetic field, an effective superconducting thickness of $t_{eff} \approx 3.4$ nm is extracted. We also performed inverse Fourier transforms of the in-plane interference pattern (see section S9), and the obtained current density profile shows that the supercurrent is uniformly distributed through the top ~5 nm of the flake, which is in quite good agreement with t_{eff}. These results imply that only a thin layer on the top of the flake is being proximitized, as expected; the superconducting order is not extending deeply along the *c* axis across the layers and is markedly longer in the *ab* plane. This thin proximitized layer is reasonable for $K_{1-x}V_3Sb_5$ due to its layered structure, which is expected to be electronically anisotropic (the *c* axis versus the *ab* plane) like its sister material, CsV_3Sb_5, that has shown out-of-plane resistivity 600× larger than that in in-plane (*14*). This results in a small coherence length along the *c* axis, just like other layered materials including WTe_2 (*65*).

The interference pattern for the out-of-plane magnetic field, however, with fast oscillations on top of the background is not a typical Fraunhofer pattern. The SQUID-like fast oscillation maintains a period of ΔB~0.5 mT that is consistent with the frequency of the oscillation on the *R* versus *B* curves and corresponds to an effective flux-penetration area of $S_{eff} \sim 4.13$ μm^2 calculated from $\Phi_0 = \Delta B \cdot S_{eff}$. This is smaller than the crystal area ($S = L \cdot W \approx 12$ μm^2), which is likely caused by partial penetration of the flux, as was seen with $MoTe_2$ (*66*). The most important feature of the fast oscillation is that it is nonvanishing and survives to higher field than the main interference pattern, as shown in Fig. 4B. This long-lived, fast oscillation cannot be induced by the bulk Josephson current. Moreover, it presents a scalloped peak profile with clear excitation branches trailing from the scalloped boundary, and prominent jumps between oscillation branches are observed (Fig. 4C). This scalloped profile and excitation branches of a nonvanishing fast mode are important signatures of nonbulk, spatially localized states (i.e., not uniformly distributed supercurrent) like surface or edge states (*40*, *66*, *67*). For an enclosed area bounded by the sides of the sample, the requirement of flux quantization results in a sawtooth profile of the surface Fermi velocity, which contributes to the scalloped profile and excitation branches, as observed in the edge state of $MoTe_2$ (*66*). We also performed inverse Fraunhofer transform for the out-of-plane field interference pattern to extract the supercurrent density distribution along the width direction, and, although the quantitative analysis has some error due to the complicated I_c versus *B* pattern, the existence of two clear peaks in the current profile qualitatively indicates the presence of edge supercurrent (see details in fig. S11).

To examine the origin of this edge supercurrent, we further performed density functional theory (DFT) calculations of the electronic band structure of KV_3Sb_5. Previous works on both the isostructural and isoelectronic compounds CsV_3Sb_5 and KV_3Sb_5 have predicted $\mathbb{Z}_2$-protected topological surface Dirac crossings just above the Fermi level (*14*, *15*). Here, we calculated the spectral density of bulk (top panel) and surface states (bottom panel) particularly on the (100)/(010) planes (*ac*/*bc* planes), including states propagating along the [001] directions, as results shown in Fig. 4D. Although the large number of surface states prevents us from attributing the surface conductivity to a single surface band, our calculations show that there are prominent surface states near the Fermi level along the $\overline{X} - \overline{M}$ line, and the Fermi level of $K_{1-x}V_3Sb_5$ [slightly below the predicted level, as shown by previous angle-resolved photoemission spectroscopy (ARPES) measurements (*18*)] cuts the surface states near the $\overline{X}$ point (corresponding to the edges in our thin flake JJ device). These surface states should contribute to the edge supercurrent shown as SQUID-like fast oscillations in the $K_{1-x}V_3Sb_5$ JJ. See Methods and section S10 for more details of surface states. It should be noted that the surface states in the *ab* plane were not detected when applying in-plane field along the *y* axis, because only the top layers of the $K_{1-x}V_3Sb_5$ samples were proximitized; coupling between the top and bottom surface states to result in the SQUID-like pattern was not possible, in analogy to what was seen with the hinge states in Al_2O_3 back-filled WTe_2 devices (*68*). Detecting the *ab*-plane surface states is an area for future work and will require very thin flakes (sub–10 nm) or vertical JJ architectures.

In summary, we fabricated JJs of the topological Kagome metal, $K_{1-x}V_3Sb_5$, and observed Josephson coupling through long distance; asymmetry and reversion of *R* versus *B* as well as a zero-field minimum in the I_c versus *B* pattern, which indicate anisotropic internal magnetism and possible spin-triplet superconductivity; and also the signal of supercurrent of the predicted topological surface states in $K_{1-x}V_3Sb_5$. These observations in one system open the door for exploring emergent physical phenomena combination of superconductivity with unconventional charge order state and topology. Fundamentally, there is a variety of opportunities for future theoretical and experimental work to excavate unconventional superconductivity based on JJs of Kagome materials.

METHODS

Device fabrication and measurement

Thin flakes of KV_3Sb_5 were exfoliated onto an SiO_2/Si substrate, followed by standard electron beam lithography and sputtering processes to fabricate the JJ devices with Niobium (~ 40 nm) as the superconducting electrodes. The JJs were measured in a Bluefors dilution refrigerator with base temperature reaching ~15 mK. The resistance of device was measured by applying different ac current excitations with low frequencies (below 30 Hz) and Zurich lock-

Downloaded from https://www.science.org at Delft University on July 24, 2023

in amplifiers. The differential resistance (dV/dI) was measured by adding an external dc source onto the small ac source of lock-in.

DFT calculations

The electronic structure of KV_3Sb_5 was simulated in Vienna Ab-initio Simulation Package (VASP) v5.4.4 (*69*–*71*) using projector-augmented wave (PAW) potentials (*72*, *73*) with identical parameters to a previous work on CsV_3Sb_5 (*14*). Calculations used the Perdew-Burke-Ernzerhof (PBE) functional (*74*) with D3 dispersion corrections (*75*), a Γ-centered 11 × 11 × 5 k-mesh, a plane wave energy cutoff of 500 eV, and the recommended PAW potentials for v5.2. No magnetic moments were incorporated in the simulation. a and c lattice parameters of the relaxed cell were 5.42 and 8.92 Å, which are in good agreement with experimental lattice parameters of 5.48 and 8.95 Å, respectively. Similar PBE functional calculations have been shown to accurately recreate the slab electronic structure measured in ARPES experiments for both CsV_3Sb_5 (*14*) and KV_3Sb_5 (*18*). Wannier90 was used to generate an empirical tight-binding model starting from initial projectors corresponding to valence orbitals (V p, d; Sb p; with a frozen inner fitting window of Fermi energy $E_F \pm 2$ eV and an outer window of $E_F - 6$ eV to $E_F + 5$ eV) (*76*). Surface density–of–state calculations were performed using the method of Sancho and coworkers (*77*) as implemented in WannierTools (*78*).

Calculation of coherence length

For $K_{1-x}V_3Sb_5$, according to equation $\mu = el_e/\hbar k_F$ with mobility $\mu \sim 0.2\ m^2/Vs$ (*18*) and $k_F \sim 0.032\ Å^{-1}$, the mean free path of $l_e \sim 42$ nm is extracted. Because l_e is smaller than the coherence length of Nb ($\xi_S = \frac{\hbar V_F}{1.76\pi k_B T_c} \approx 64$ nm, $T_c \approx 6.2$ K, $V_F \approx 3 \times 10^5$ m/s) (*79*), the superconducting coherence length of spin-singlet pairing in nonmagnetic materials (*53*, *65*) or spin-triplet pairs in a magnetic system (*49*) can be calculated by $\xi_N = \sqrt{\hbar v_F l_e / 6\pi k_B T_c}$ (Fermi velocity $v_F \sim 3.77 \times 10^5$ m/s, $T_c \sim 0.78$ K), which is about 230 nm in $K_{1-x}V_3Sb_5$.

Supplementary Materials

This PDF file includes:

Sections S1 to S10
Figs. S1 to S14

REFERENCES AND NOTES

1. M. R. Norman, Colloquium: Herbertsmithite and the search for the quantum spin liquid. *Rev. Mod. Phys.* **88**, 041002 (2016).
2. M. L. Kiesel, C. Platt, R. Thomale, Unconventional fermi surface instabilities in the kagome hubbard model. *Phys. Rev. Lett.* **110**, 126405 (2013).
3. L. Balents, Spin liquids in frustrated magnets. *Nature* **464**, 199–208 (2010).
4. S. Baidya, A. V. Mallik, S. Bhattacharjee, T. Saha-Dasgupta, Interplay of magnetism and topological superconductivity in bilayer kagome metals. *Phys. Rev. Lett.* **125**, 026401 (2020).
5. L. Ye, M. Kang, J. Liu, F. Von Cube, C. R. Wicker, T. Suzuki, C. Jozwiak, A. Bostwick, E. Rotenberg, D. C. Bell, L. Fu, R. Comin, J. G. Checkelsky, Massive Dirac fermions in a ferromagnetic kagome metal. *Nature* **555**, 638–642 (2018).
6. D. F. Liu, A. J. Liang, E. K. Liu, Q. N. Xu, Y. W. Li, C. Chen, D. Pei, W. J. Shi, S. K. Mo, P. Dudin, T. Kim, C. Cacho, G. Li, Y. Sun, L. X. Yang, Z. K. Liu, S. S. P. Parkin, C. Felser, Y. L. Chen, Magnetic Weyl semimetal phase in a Kagomé crystal. *Science* **365**, 1282–1285 (2019).
7. B. R. Ortiz, L. C. Gomes, J. R. Morey, M. Winiarski, M. Bordelon, J. S. Mangum, I. W. H. Oswald, J. A. Rodriguez-Rivera, J. R. Neilson, S. D. Wilson, E. Ertekin, T. M. McQueen, E. S. Toberer, New kagome prototype materials: Discovery of KV_3Sb_5,RbV_3Sb_5, and CsV_3Sb_5. *Phys. Rev. Mater.* **3**, 094407 (2019).
8. T. Neupert, M. M. Denner, J.-X. Yin, R. Thomale, M. Z. Hasan, Charge order and superconductivity in kagome materials. *Nat. Phys.* **18**, 137–143 (2022).
9. Y. X. Jiang, J. X. Yin, M. M. Denner, N. Shumiya, B. R. Ortiz, G. Xu, Z. Guguchia, J. He, M. S. Hossain, X. Liu, J. Ruff, L. Kautzsch, S. S. Zhang, G. Chang, I. Belopolski, Q. Zhang, T. A. Cochran, D. Multer, M. Litskevich, Z. J. Cheng, X. P. Yang, Z. Wang, R. Thomale, T. Neupert, S. D. Wilson, M. Z. Hasan, Unconventional chiral charge order in kagome superconductor KV_3Sb_5. *Nat. Mater.* **20**, 1353–1357 (2021).
10. B. R. Ortiz, S. M. L. Teicher, L. Kautzsch, P. M. Sarte, N. Ratcliff, J. Harter, J. P. C. Ruff, R. Seshadri, S. D. Wilson, Fermi surface mapping and the nature of charge-density-wave order in the kagome superconductor CsV_3Sb_5. *Phys. Rev. X.* **11**, 041030 (2021).
11. H. Chen, H. Yang, B. Hu, Z. Zhao, J. Yuan, Y. Xing, G. Qian, Z. Huang, G. Li, Y. Ye, S. Ma, S. Ni, H. Zhang, Q. Yin, C. Gong, Z. Tu, H. Lei, H. Tan, S. Zhou, C. Shen, X. Dong, B. Yan, Z. Wang, H. J. Gao, Roton pair density wave in a strong-coupling kagome superconductor. *Nature* **599**, 222–228 (2021).
12. H. Zhao, H. Li, B. R. Ortiz, S. M. L. Teicher, T. Park, M. Ye, Z. Wang, L. Balents, S. D. Wilson, I. Zeljkovic, Cascade of correlated electron states in the kagome superconductor CsV_3Sb_5. *Nature* **599**, 216–221 (2021).
13. Z. Wang, Y. X. Jiang, J. X. Yin, Y. Li, G. Y. Wang, H. L. Huang, S. Shao, J. Liu, P. Zhu, N. Shumiya, M. S. Hossain, H. Liu, Y. Shi, J. Duan, X. Li, G. Chang, P. Dai, Z. Ye, G. Xu, Y. Wang, H. Zheng, J. Jia, M. Z. Hasan, Y. Yao, Electronic nature of chiral charge order in the kagome superconductor CsV_3Sb_5. *Phys. Rev. B.* **104**, 075148 (2021).
14. B. R. Ortiz, S. M. L. Teicher, Y. Hu, J. L. Zuo, P. M. Sarte, E. C. Schueller, A. M. M. Abeykoon, M. J. Krogstad, S. Rosenkranz, R. Osborn, R. Seshadri, L. Balents, J. He, S. D. Wilson, CsV_3Sb_5: A Z_2 topological kagome metal with a superconducting ground state. *Phys. Rev. Lett.* **125**, 247002 (2020).
15. B. R. Ortiz, P. M. Sarte, E. M. Kenney, M. J. Graf, S. M. L. Teicher, R. Seshadri, S. D. Wilson, Superconductivity in the Z_2 kagome metal KV_3Sb_5. *Phys. Rev. Mater.* **5**, 034801 (2021).
16. Z. Liang, X. Hou, F. Zhang, W. Ma, P. Wu, Z. Zhang, F. Yu, J. J. Ying, K. Jiang, L. Shan, Z. Wang, X. H. Chen, Three-dimensional charge density wave and surface-dependent vortex-core states in a kagome superconductor CsV_3Sb_5. *Phys. Rev. X.* **11**, 031026 (2021).
17. Y. Xiang, Q. Li, Y. Li, W. Xie, H. Yang, Z. Wang, Y. Yao, H. H. Wen, Twofold symmetry of c-axis resistivity in topological kagome superconductor CsV_3Sb_5 with in-plane rotating magnetic field. *Nat. Commun.* **12**, 6727 (2021).
18. S. Y. Yang, Y. Wang, B. R. Ortiz, D. Liu, J. Gayles, E. Derunova, R. Gonzalez-Hernandez, L. Šmejkal, Y. Chen, S. S. P. Parkin, S. D. Wilson, E. S. Toberer, T. McQueen, M. N. Ali, Giant, unconventional anomalous Hall effect in the metallic frustrated magnet candidate, KV_3Sb_5. *Sci. Adv.* **6**, eabb6003 (2020).
19. F. H. Yu, T. Wu, Z. Y. Wang, B. Lei, W. Z. Zhuo, J. J. Ying, X. H. Chen, Concurrence of anomalous hall effect and charge density wave in a superconducting topological kagome metal. *Phys. Rev. B.* **104**, L041103 (2021).
20. Y. Hu, X. Wu, B. R. Ortiz, S. Ju, X. Han, J. Ma, N. C. Plumb, M. Radovic, R. Thomale, S. D. Wilson, A. P. Schnyder, M. Shi, Rich nature of Van Hove singularities in Kagome superconductor CsV_3Sb_5. *Nat. Commun.* **13**, 2220 (2022).
21. M. Kang, S. Fang, J. K. Kim, B. R. Ortiz, S. H. Ryu, J. Kim, J. Yoo, G. Sangiovanni, D. Di Sante, B. G. Park, C. Jozwiak, A. Bostwick, E. Rotenberg, E. Kaxiras, S. D. Wilson, J. H. Park, R. Comin, Twofold van Hove singularity and origin of charge order in topological kagome superconductor CsV_3Sb_5. *Nat. Phys.* **18**, 301–308 (2022).
22. C. Mielke 3rd, D. Das, J.-X. Yin, H. Liu, R. Gupta, Y. X. Jiang, M. Medarde, X. Wu, H. C. Lei, J. Chang, P. Dai, Q. Si, H. Miao, R. Thomale, T. Neupert, Y. Shi, R. Khasanov, M. Z. Hasan, H. Luetkens, Z. Guguchia, Time-reversal symmetry-breaking charge order in a kagome superconductor. *Nature* **602**, 245–250 (2022).
23. R. Khasanov, D. Das, R. Gupta, C. Mielke, M. Elender, Q. Yin, Z. Tu, C. Gong, H. Lei, E. T. Ritz, R. M. Fernandes, T. Birol, Z. Guguchia, H. Luetkens, Time-reversal symmetry broken by charge order in CsV_3Sb_5. *Phys. Rev. Res.* **4**, 023244 (2022).
24. L. Yu, C. Wang, Y. Zhang, M. Sander, S. Ni, Z. Lu, S. Ma, Z. Wang, Z. Zhao, H. Chen, K. Jiang, Y. Zhang, H. Yang, F. Zhou, X. Dong, S. L. Johnson, M. J. Graf, J. Hu, H.-J. Gao, Z. Zhao, Evidence of a hidden flux phase in the topological kagome metal CsV_3Sb_5. arXiv:2107.10714 [cond-mat.supr-con] (2021).
25. H. Li, H. Zhao, B. R. Ortiz, T. Park, M. Ye, L. Balents, Z. Wang, S. D. Wilson, I. Zeljkovic, Rotation symmetry breaking in the normal state of a kagome superconductor KV_3Sb_5. *Nat. Phys.* **18**, 265–270 (2022).
26. Q. Wu, Z. X. Wang, Q. M. Liu, R. S. Li, S. X. Xu, Q. W. Yin, C. S. Gong, Z. J. Tu, H. C. Lei, T. Dong, N. L. Wang, Simultaneous formation of two-fold rotation symmetry with charge order in the kagome superconductor CsV_3Sb_5 by optical polarization rotation measurement. *Phys. Rev. B.* **106**, 205109 (2022).

Downloaded from https://www.science.org at Delft University on July 24, 2023

27. Y. Xu, Z. Ni, Y. Liu, B. R. Ortiz, Q. Deng, S. D. Wilson, B. Yan, L. Balents, L. Wu, Three-state nematicity and magneto-optical Kerr effect in the charge density waves in kagome superconductors. *Nat. Phys.* **18**, 1470–1475 (2022).
28. X. Wu, T. Schwemmer, T. Müller, A. Consiglio, G. Sangiovanni, D. Di Sante, Y. Iqbal, W. Hanke, A. P. Schnyder, M. M. Denner, M. H. Fischer, T. Neupert, R. Thomale, Nature of unconventional pairing in the kagome superconductors AV_3Sb_5 (A = K, Rb, Cs). *Phys. Rev. Lett.* **127**, 177001 (2021).
29. E. Uykur, B. R. Ortiz, S. D. Wilson, M. Dressel, A. A. Tsirlin, Optical detection of the density-wave instability in the kagome metal KV_3Sb_5. *npj Quantum Mater.* **7**, 16 (2022).
30. X. Feng, Y. Zhang, K. Jiang, J. Hu, Low-energy effective theory and symmetry classification of flux phases on the kagome lattice. *Phys. Rev. B.* **104**, 165136 (2021).
31. T. Park, M. Ye, L. Balents, Electronic instabilities of kagome metals: Saddle points and Landau theory. *Phys. Rev. B.* **104**, 035142 (2021).
32. X. Feng, K. Jiang, Z. Wang, J. Hu, Chiral flux phase in the Kagome superconductor AV_3Sb_5. *Sci. Bull. (Beijing)* **66**, 1384–1388 (2021).
33. H. Tan, Y. Liu, Z. Wang, B. Yan, Charge density waves and electronic properties of superconducting kagome metals. *Phys. Rev. Lett.* **127**, 046401 (2021).
34. M. M. Denner, R. Thomale, T. Neupert, Analysis of charge order in the kagome metal AV_3Sb_5 (A= K,Rb,Cs). *Phys. Rev. Lett.* **127**, 217601 (2021).
35. H. D. Scammell, J. Ingham, T. Li, O. P. Sushkov, Chiral excitonic order from twofold van Hove singularities in kagome metals. *Nat. Commun.* **14**, 605 (2023).
36. E. M. Kenney, B. R. Ortiz, C. Wang, S. D. Wilson, M. J. Graf, Absence of local moments in the kagome metal KV_3Sb_5 as determined by muon spin spectroscopy. *J. Phys. Condens. Matter* **33**, 235801 (2021).
37. H. Li, S. Wan, H. Li, Q. Li, Q. Gu, H. Yang, Y. Li, Z. Wang, Y. Yao, H. H. Wen, No observation of chiral flux current in the topological kagome metal CsV_3Sb_5. *Phys. Rev. B.* **105**, 045102 (2022).
38. C. Mu, Q. Yin, Z. Tu, C. Gong, H. Lei, Z. Li, J. Luo, S-wave superconductivity in kagome metal CsV_3Sb_5 revealed by $^{121/123Sb}$NQR and ^{51}V NMR measurements. *Chinese Phys. Lett.* **38**, 077402 (2021).
39. M. Veldhorst, M. Snelder, M. Hoek, T. Gang, V. K. Guduru, X. L. Wang, U. Zeitler, W. G. Van Der Wiel, A. A. Golubov, H. Hilgenkamp, A. Brinkman, Josephson supercurrent through a topological insulator surface state. *Nat. Mater.* **11**, 417–421 (2012).
40. S. Hart, H. Ren, T. Wagner, P. Leubner, M. Mühlbauer, C. Brüne, H. Buhmann, L. W. Molenkamp, A. Yacoby, Induced superconductivity in the quantum spin Hall edge. *Nat. Phys.* **10**, 638–643 (2014).
41. W. Han, S. Maekawa, X. C. Xie, Spin current as a probe of quantum materials. *Nat. Mater.* **19**, 139–152 (2020).
42. M. Eschrig, Spin-polarized supercurrents for spintronics. *Phys. Today* **64**, 43–49 (2011).
43. J. Linder, J. W. A. Robinson, Superconducting spintronics. *Nat. Phys.* **11**, 307–315 (2015).
44. N. O. Birge, Spin-triplet supercurrents in Josephson junctions containing strong ferromagnetic materials. *Philos. Trans. R. Soc. A Math. Phys. Eng. Sci.* **376**, 20150150 (2018).
45. R. S. Keizer, S. T. B. Goennenwein, T. M. Klapwijk, G. Miao, G. Xiao, A. Gupta, A spin triplet supercurrent through the half-metallic ferromagnet CrO_2. *Nature* **439**, 825–827 (2006).
46. J. W. A. Robinson, J. D. S. Witt, M. G. Blamire, Controlled injection of spin-triplet supercurrents into a strong ferromagnet. *Science* **329**, 59–61 (2010).
47. M. Eschrig, T. Löfwander, Triplet supercurrents in clean and disordered half-metallic ferromagnets. *Nat. Phys.* **4**, 138–143 (2008).
48. T. S. Khaire, M. A. Khasawneh, W. P. Pratt, N. O. Birge, Observation of spin-triplet superconductivity in co-based josephson junctions. *Phys. Rev. Lett.* **104**, 137002 (2010).
49. T. Nakamura, L. D. Anh, Y. Hashimoto, S. Ohya, M. Tanaka, S. Katsumoto, Evidence for spin-triplet electron pairing in the proximity-induced superconducting state of an Fe-doped in as semiconductor. *Phys. Rev. Lett.* **122**, 107001 (2019).
50. H. Ren, F. Pientka, S. Hart, A. T. Pierce, M. Kosowsky, L. Lunczer, R. Schlereth, B. Scharf, E. M. Hankiewicz, L. W. Molenkamp, B. I. Halperin, A. Yacoby, Topological superconductivity in a phase-controlled Josephson junction. *Nature* **569**, 93–98 (2019).
51. S. M. Frolov, M. J. Manfra, J. D. Sau, Topological superconductivity in hybrid devices. *Nat. Phys.* **16**, 718–724 (2020).
52. P. Dubos, H. Courtois, B. Pannetier, F. K. Wilhelm, A. D. Zaikin, G. Schön, Josephson critical current in a long mesoscopic S-N-S junction. *Phys. Rev. B.* **63**, 064502 (2001).
53. I. Bozovic, G. Logvenov, M. A. J. Verhoeven, P. Caputo, E. Goldobin, M. R. Beasley, Giant proximity effect in cuprate superconductors. *Phys. Rev. Lett.* **93**, 157002 (2004).
54. L. Covaci, F. Marsiglio, Proximity effect and Josephson current in clean strong/weak/strong superconducting trilayers. *Phys. Rev. B.* **73**, 014503 (2006).
55. A. Kononov, G. Abulizi, K. Qu, J. Yan, D. Mandrus, K. Watanabe, T. Taniguchi, C. Schönenberger, One-dimensional edge transport in few-layer WTe_2. *Nano Lett.* **20**, 4228–4233 (2020).
56. O. O. Shvetsov, V. D. Esin, Y. S. Barash, A. V. Timonina, N. N. Kolesnikov, E. V. Deviatov, Lateral Josephson effect on the surface of the magnetic Weyl semimetal $Co_3Sn_2S_2$. *Phys. Rev. B.* **101**, 035304 (2020).
57. Y. Hu, S. Yamane, G. Mattoni, K. Yada, K. Obata, Y. Li, Y. Yao, Z. Wang, J. Wang, C. Farhang, J. Xia, Y. Maeno, S. Yonezawa, Time-reversal symmetry breaking in charge density wave of CsV3Sb5 detected by polar Kerr effect. arXiv:2208.08036 [cond-mat.str-el] (2022).
58. Z. Guguchia, C. Mielke III, D. Das, R. Gupta, J.-X. Yin, H. Liu, Q. Yin, M. H. Christensen, Z. Tu, C. Gong, N. Shumiya, T. Gamsakhurdashvili, M. Elender, P. Dai, A. Amato, Y. Shi, H. C. Lei, R. M. Fernandes, M. Z. Hasan, H. Luetkens, R. Khasanov, Tunable unconventional kagome superconductivity in charge ordered RbV_3Sb_5 and KV_3Sb_5. *Nat. Commun.* **14**, 153 (2023).
59. A. Iovan, T. Golod, V. M. Krasnov, Controllable generation of a spin-triplet supercurrent in a Josephson spin valve. *Phys. Rev. B.* **90**, 134514 (2014).
60. J. F. Liu, K. S. Chan, Anomalous Josephson current through a ferromagnetic trilayer junction. *Phys. Rev. B.* **82**, 184533 (2010).
61. N. Banerjee, J. W. A. Robinson, M. G. Blamire, Reversible control of spin-polarized supercurrents in ferromagnetic Josephson junctions. *Nat. Commun.* **5**, 4771 (2014).
62. S. L. Yu, J. X. Li, Chiral superconducting phase and chiral spin-density-wave phase in a Hubbard model on the kagome lattice. *Phys. Rev. B.* **85**, 144402 (2012).
63. R. Tazai, Y. Yamakawa, S. Onari, H. Kontani, Mechanism of exotic density-wave and beyond-Migdal unconventional superconductivity in kagome metal AV_3Sb_5 (A = K, Rb, Cs). *Sci. Adv.* **8**, eabl4108 (2022).
64. A. T. Rømer, S. Bhattacharyya, R. Valentí, M. H. Christensen, B. M. Andersen, Superconductivity from repulsive interactions on the kagome lattice. *Phys. Rev. B.* **106**, 174514 (2022).
65. Q. Li, C. He, Y. Wang, E. Liu, M. Wang, Y. Wang, J. Zeng, Z. Ma, T. Cao, C. Yi, N. Wang, K. Watanabe, T. Taniguchi, L. Shao, Y. Shi, X. Chen, S. J. Liang, Q. H. Wang, F. Miao, Proximity-induced superconductivity with subgap anomaly in type II Weyl semi-metal WTe_2. *Nano Lett.* **18**, 7962–7968 (2018).
66. W. Wang, S. Kim, M. Liu, F. A. Cevallos, R. J. Cava, N. P. Ong, Evidence for an edge supercurrent in the Weyl superconductor $MoTe_2$. *Science* **368**, 534–537 (2020).
67. F. Schindler, Z. Wang, M. G. Vergniory, A. M. Cook, A. Murani, S. Sengupta, A. Y. Kasumov, R. Deblock, S. Jeon, I. Drozdov, H. Bouchiat, S. Guéron, A. Yazdani, B. A. Bernevig, T. Neupert, Higher-order topology in bismuth. *Nat. Phys.* **14**, 918–924 (2018).
68. Y.-B. Choi, Y. Xie, C.-Z. Chen, J. Park, S.-B. Song, J. Yoon, B. J. Kim, T. Taniguchi, K. Watanabe, J. Kim, K. C. Fong, M. N. Ali, K. T. Law, G.-H. Lee, Evidence of higher-order topology in multilayer WTe_2 from Josephson coupling through anisotropic hinge states. *Nat. Mater.* **19**, 974–979 (2020).
69. G. Kresse, J. Hafner, Ab initio molecular-dynamics simulation of the liquid-metal–amorphous-semiconductor transition in germanium. *Phys. Rev. B.* **49**, 14251–14269 (1994).
70. G. Kresse, J. Furthmüller, Efficient iterative schemes for ab initio total-energy calculations using a plane-wave basis set. *Phys. Rev. B. Condens. Matter.* **54**, 11169–11186 (1996).
71. G. Kresse, J. Furthmüller, Efficiency of ab-initio total energy calculations for metals and semiconductors using a plane-wave basis set. *Comput. Mater. Sci.* **6**, 15–50 (1996).
72. P. E. Blöchl, Projector augmented-wave method. *Phys. Rev. B.* **50**, 17953–17979 (1994).
73. D. Joubert, From ultrasoft pseudopotentials to the projector augmented-wave method. *Phys. Rev. B.* **59**, 1758–1775 (1999).
74. J. P. Perdew, K. Burke, M. Ernzerhof, Generalized gradient approximation made simple. *Phys. Rev. Lett.* **77**, 3865–3868 (1996).
75. S. Grimme, S. Ehrlich, L. Goerigk, Effect of the damping function in dispersion corrected density functional theory. *J. Comput. Chem.* **32**, 1456 (2011).
76. A. A. Mostofi, J. R. Yates, G. Pizzi, Y. S. Lee, I. Souza, D. Vanderbilt, N. Marzari, An updated version of wannier90: A tool for obtaining maximally-localised Wannier functions. *Comput. Phys. Commun.* **185**, 2309–2310 (2014).
77. M. P. Lopez Sancho, J. M. Lopez Sancho, J. Rubio, Highly convergent schemes for the calculation of bulk and surface Green functions. *J. Phys. F Met. Phys.* **15**, 851–858 (1985).
78. Q. S. Wu, S. N. Zhang, H. F. Song, M. Troyer, A. A. Soluyanov, WannierTools: An open-source software package for novel topological materials. *Comput. Phys. Commun.* **224**, 405–416 (2018).
79. A. V. Pronin, M. Dressel, A. Pimenov, A. Loidl, I. V. Roshchin, L. H. Greene, Direct observation of the superconducting energy gap developing in the conductivity spectra of niobium. *Phys. Rev. B.* **57**, 14416–14421 (1998).

Acknowledgments: We thank F. Gao and J.-C. Jeon for the support during device fabrication and G.-H. Lee and V. K. T. Law and for valuable discussions. **Funding:** M.N.A. acknowledges that this research was principally supported by the Alexander von Humboldt Foundation Sofia Kovalevskaja Award, the German Federal Ministry of Education and Research's MINERVA ARCHES Award, and the Max Planck Society. Y.W. acknowledges the support from NWO Talent Programme Veni financed by the Dutch Research Council (NWO), project no. VI.Veni.212.146. S.D.W., B.R.O., and S.M.L.T. acknowledge support from the University of California Santa Barbara

Downloaded from https://www.science.org at Delft University on July 24, 2023

Quantum Foundry, funded by the National Science Foundation (NSF DMR-1906325). Research reported here also made use of shared facilities of the UCSB MRSEC (NSF DMR-1720256). B.R.O. also acknowledges support from the California NanoSystems Institute through the Elings fellowship program. S.M.L.T. has been supported by the National Science Foundation Graduate Research Fellowship Program under grant no. DGE-1650114. Any opinions, findings, and conclusions or recommendations expressed in this material are those of the authors and do not necessarily reflect the views of the National Science Foundation. D.L. acknowledges support from the Alexander von Humboldt Foundation. S.S.P.P. acknowledges the European Research Council (ERC) under the European Union's Horizon 2020 research and innovation programme (grant agreement no. 670166), Deutsche Forschungsgemeinschaft (DFG, German Research Foundation)—project number 314790414, and Alexander von Humboldt Foundation in the framework of the Alexander von Humboldt Professorship endowed by the Federal Ministry of Education and Research. T.M. acknowledges the David and Lucile Packard Foundation and the Johns Hopkins University Catalyst Award. E.S.T. acknowledges support of NSF DMR 1555340.

Author contributions: Y.W. and M.N.A. conceived and designed the study. B.R.O. grew the samples. Y.W. and S.-Y.Y. fabricated the devices. Y.W., P.K.S., and S.-Y.Y. performed the transport measurement. Y.W., H.W., S.-Y.Y., C.G., and D.L. carried out the data analysis. S.M.L.T. carried out DFT calculations and theoretical analysis. A.K.S. performed the energy-dispersive x-ray measurements. E.S.T., T.M., S.D.W., and M.N.A. are the principal investigators. All authors contributed to the preparation of manuscript. **Competing interests:** The authors declare that they have no competing interests. **Data and materials availability:** All data needed to evaluate the conclusions in the paper are present in the paper and/or the Supplementary Materials.

Submitted 17 January 2023
Accepted 12 June 2023
Published 12 July 2023
10.1126/sciadv.adg7269

Downloaded from https://www.science.org at Delft University on July 24, 2023

ScienceAdvances

Anisotropic proximity–induced superconductivity and edge supercurrent in Kagome metal, $K_{1-x}V_3Sb_5$

Yaojia Wang, Shuo-Ying Yang, Pranava K. Sivakumar, Brenden R. Ortiz, Samuel M. L. Teicher, Heng Wu, Abhay K. Srivastava, Chirag Garg, Defa Liu, Stuart S. P. Parkin, Eric S. Toberer, Tyrel McQueen, Stephen D. Wilson, and Mazhar N. Ali

Sci. Adv., **9** (28), eadg7269.
DOI: 10.1126/sciadv.adg7269

View the article online
https://www.science.org/doi/10.1126/sciadv.adg7269
Permissions
https://www.science.org/help/reprints-and-permissions

Downloaded from https://www.science.org at Delft University on July 24, 2023

Use of this article is subject to the Terms of service

Science Advances (ISSN) is published by the American Association for the Advancement of Science. 1200 New York Avenue NW, Washington, DC 20005. The title *Science Advances* is a registered trademark of AAAS.
Copyright © 2023 The Authors, some rights reserved; exclusive licensee American Association for the Advancement of Science. No claim to original U.S. Government Works. Distributed under a Creative Commons Attribution License 4.0 (CC BY).